Research Article

Parametric Investigation of Dual-Mass Flywheel Based on Driveline Start-Up Torsional Vibration Control

Liupeng He [ID],[1] Changgao Xia [ID],[1] Sida Chen,[1] Jiwei Guo,[2] and Yi Liu[2]

[1]*School of Automotive and Traffic Engineering, Jiangsu University, Zhenjiang 212013, China*
[2]*Shanghai Sachs Powertrain Components Systems Co. Ltd., Shanghai 201799, China*

Correspondence should be addressed to Changgao Xia; xiacg@ujs.edu.cn

This paper is aimed to investigate the influence of dual-mass flywheel (DMF) kinetic parameters on driveline torsional vibration in engine start-up process, which prescribes the design requirements under start-up condition for DMF matching. On the basis of driveline excitation analysis during engine start-up, the analytical model of DMF driveline torsional vibration system is built and simulated. The vehicle start-up test is conducted and compared with the simulation results. On account of the partial nonstationary characteristic of driveline during start-up, the start-up process is separated into 3 phases for discussing the influence of DMF rotary inertia ratio, hysteresis torque, and nonlinear torsional stiffness on attenuation effect. The test and simulation results show that the DMF undergoes severe oscillation when driveline passes through resonance zone, and the research model is verified to be valid. The DMF design requirements under start-up condition are obtained: the appropriate rotary inertia ratio (the 1st flywheel rotary inertia-to-the 2nd flywheel rotary inertia ratio) is 0.7~1.1; the interval of DMF small torsion angle should be designed as being with small damping, while large damping is demanded in the interval of large torsion angle; DMF should be equipped with low torsional stiffness when working in start-up process.

1. Introduction

The torsional vibration of vehicle powertrain system is a direct excitation source of vehicle driveline noise and body vibration, reducing driving comfort. Better driveline torsional vibration control is demanded due to the stronger engine output torque and widely used diesel engine presently.

The traditional clutch torsional damper (CTD) cannot meet the requirements for torsional vibration control presently, since many defects have been proved [1], e.g., driveline resonance at idle speed or commonly used speed. The dual-mass flywheel torsional vibration damper (DMF) separates the flywheel into two components, the primary flywheel and the secondary flywheel, which are connected by springs and damping mechanism [2]. Compared to CTD, DMF has larger relative rotation angle, lower torsional stiffness, and better performance in torque

transmission. Meanwhile, DMF can effectively reduce the low-order natural frequency of driveline [3], attenuating driveline torsional vibration. DMF plays an active role in absorbing driveline oscillation, mitigating driveline impact, reducing fuel consumption [3–6], etc.

Many studies have been carried out regarding DMF characteristics since the 1980s, when DMF was invented, and the research studies of Luk company are prominent [7, 8]. Hu et al. established the undamped torsional vibration model and researched the influence of DMF on driveline natural characteristics under idling and driving conditions [9]. Schweinfurt of ZF Company investigated the damping effect of DMF by analyzing the angular acceleration of the secondary flywheel based on the DMF dynamic model that utilized single frequency vibration as input in Simulink software [10]. Chen et al. established the 8-degree-of-freedom model of idle condition and the 12-degree-of-freedom model of driving condition by MSC's Easy5

software. The influences of DMF parameters on driveline natural characteristics and vibration control under driving condition were investigated [11]. Wang et al. studied the DMF parameters matching and design method based on driving and overload conditions at different engaged gear pairs, and a DMF with 3-stage torsional stiffness was designed [12]. Deng and Burde investigated the relationship between the engine starter characteristics and driveline resonance frequency [13]. Chen et al. simulated the dynamic characteristics of DMF-CS (DMF with circumferential spring). The results showed that the powertrain system bears large vibration under start-up and stop conditions. It was suggested that the torsional vibration amplitude could be decreased by increasing DMF damping [14].

The literatures have made achievements in DMF matching based on vibration control under idling and driving conditions. However, the DMF design requirements under start-up condition remain to be discussed and analyzed. The resonant speed of DMF driveline is under idle speed, which indicates that the driveline will pass through the resonance speed in start-up process inevitably. Severe oscillation of vehicle and DMF or even the damage of DMF will occur under resonance condition [14]. Consequently, the vibration control under start-up condition should be considered necessarily in the process of DMF matching.

Based on the previous studies, the current paper models and tests DMF driveline system under start-up condition, and the influences of DMF kinetic parameters on driveline vibration control are investigated and analyzed.

2. DMF Driveline Start-Up Analysis

As shown in Figure 1, the clutch is separated from the gearbox and drive axle in start-up process. Hence the fuel

vehicle powertrain equipped with DMF mainly contains engine starter, engine, DMF, clutch, etc. The driveline torsional vibration is impacted by the dynamic torsional characteristics of each component.

Driveline in Figure 1 is simplified to a torsional vibration system shown in Figure 2 for analyzing DMF attenuation mechanism. The left is the equivalent rotary components at the primary flywheel side and the right is the equivalent rotary components at the secondary flywheel side.

The differential equations of torsional vibration are as follows:

$$
\begin{cases}
I_p \ddot{\theta}_p + C(\dot{\theta}_p - \dot{\theta}_s) + K_d(\theta_p - \theta_s) = T, \\
I_s \ddot{\theta}_s + C(\dot{\theta}_s - \dot{\theta}_p) + K_d(\theta_s - \theta_p) + K_s \theta_s = 0,
\end{cases}
\tag{1}
$$

where θ_p (rad) is the angular displacement of the primary side; I_p (kg·m^2) is the equivalent rotary inertia of the primary side; T (Nm) is the excitation torque, and suppose $T = T_A \cdot e^{i\omega t}$, where T_A is the torque amplitude and ω is the excitation circular frequency; K_d (Nm/rad) is the DMF torsional stiffness; C (Nms/rad) is the DMF torsional damping; θ_s (rad) is the angular displacement of the secondary side; I_s (kg·m^2) is the equivalent rotary inertia of the secondary side; and K_s (Nm/rad) is the equivalent torsional stiffness of the secondary side.

The steady state response of the secondary flywheel side gives

$$
\theta_s = \frac{T_A (K_d + i\omega C) e^{i\omega t}}{(K_d - I_p \omega^2)(K_s - I_s \omega^2) - K_d I_p \omega^2 + i\omega C [K_s - (I_p + I_s)\omega^2]}.
\tag{2}
$$

Amplitude of the angular displacement of the secondary flywheel side gives

$$
|\theta_s| = T_A \sqrt{\frac{K_d^2 + \omega^2 C^2}{[(K_d - I_p \omega^2)(K_s - I_s \omega^2) - K_d I_p \omega^2]^2 + \omega^2 C^2 [K_s - (I_p + I_s)\omega^2]^2}}.
\tag{3}
$$

Equation (3) shows that angular displacement amplitude of the secondary flywheel side is related to I_p, I_s, K_d, K_s, and C. The vehicle system parameters are previously determined before DMF matching; therefore, the attenuation effect is associated with the distribution of rotary inertia, damping, and stiffness of DMF. Equation (3) also indicates that vibratory response is associated with T_A and ω, namely, input excitation. Accordingly, it is inappropriate to utilize sinusoidal signal as excitation for studying the oscillation in start-up process on account of the partial unsteady state induced by starter input torque and engine cylinder ignition.

After all the cylinders are entirely ignited, the driveline torsional vibration is generally derived from the crankshaft

system vibration, including the torque fluctuation caused by reciprocating mechanical movement of piston and connecting rod and the variation of cylinder gas pressure [15, 16].

For a 4-cylinder 4-stroke engine, the torque caused by the reciprocating mass, T_{rm}, can be expressed as

$$
T_{rm} = -4mr^2 \zeta^2 \left[\frac{\sin 2\zeta t}{2} + \sin 4\zeta t \left(\frac{\lambda_p}{2}\right)^2 \right],
\tag{4}
$$

where m (kg) is the total mass of a single piston (piston, piston ring, and piston pin) and a partial of a single connecting rod; r (mm) is the crank radius; ζ (rad/s) is the crank
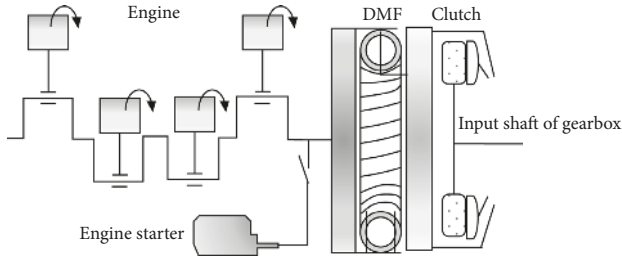
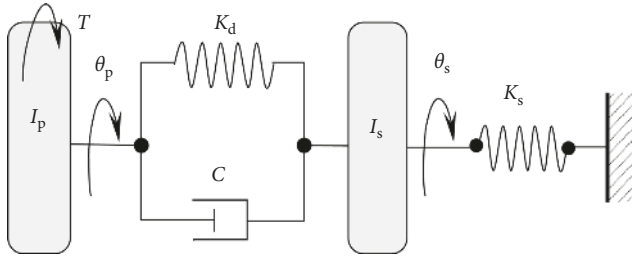FIGURE 1: Schematic drawing of DMF driveline structure under start-up condition.

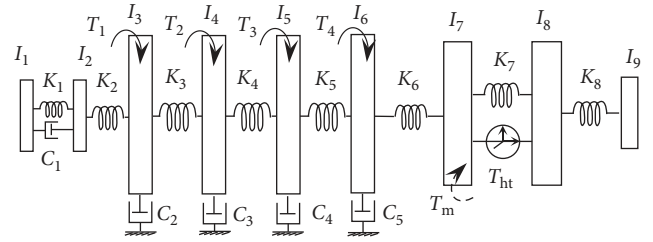FIGURE 2: 2-degree-of-freedom driveline vibration system.

FIGURE 3: Analytical model of DMF driveline under start-up condition.

initially and then disengaged from the flywheel ring gear after the engine is completely ignited.

In Figure 3, $T_1 \sim T_4$ (Nm) are the excitation torque of each cylinder, T_m (Nm) is the torque on flywheel ring gear exerted by engine starter, I_i (Kg·m^2) is the rotary inertia, K_i (Nm/rad) is torsional stiffness, and C_i (Nms/rad)) is the torsional damping coefficient, where i represents the identifier of each rotation component. T_{ht} (Nm) is the hysteresis torque of DMF. Symbol meanings are listed in Table 1.

When driveline is excited by engine starter, the kinetic equations of the driveline torsional vibration system can be expressed as follows:

$$\begin{cases} I_1\ddot{\theta}_1 + K_1(\theta_1 - \theta_2) + C_1(\dot{\theta}_1 - \dot{\theta}_2) = 0, \\ I_2\ddot{\theta}_2 + K_1(\theta_2 - \theta_1) + K_2(\theta_2 - \theta_3) + C_1(\dot{\theta}_2 - \dot{\theta}_1) = 0, \\ I_3\ddot{\theta}_3 + K_2(\theta_3 - \theta_2) + K_3(\theta_3 - \theta_4) + C_2\dot{\theta}_3 = 0, \\ I_4\ddot{\theta}_4 + K_3(\theta_4 - \theta_3) + K_4(\theta_4 - \theta_5) + C_3\dot{\theta}_4 = 0, \\ I_5\ddot{\theta}_5 + K_4(\theta_5 - \theta_4) + K_5(\theta_5 - \theta_6) + C_4\dot{\theta}_5 = 0, \\ I_6\ddot{\theta}_6 + K_5(\theta_6 - \theta_5) + K_6(\theta_6 - \theta_7) + C_5\dot{\theta}_6 = 0, \\ I_7\ddot{\theta}_7 + K_6(\theta_7 - \theta_6) + K_7(\theta_7 - \theta_8) + T_{ht} = T_m, \\ I_8\ddot{\theta}_8 + K_7(\theta_8 - \theta_7) + K_8(\theta_8 - \theta_9) - T_{ht} = 0, \\ I_9\ddot{\theta}_9 + K_8(\theta_9 - \theta_8) = 0. \end{cases}$$ (7)

According to equation (7), the matrix of excitation torque $\mathbf{T}$ can be integrated as

$$\mathbf{T} = [0, 0, 0, 0, 0, 0, T_m, 0, 0]^T.$$ (8)

When starter is disconnected from the system and engine is completely ignited, the excitation torque matrix is

$$\mathbf{T} = [0, 0, T_1, T_2, T_3, T_4, 0, 0, 0]^T.$$ (9)

Based on a testing vehicle, the model is simulated by SimulationX software [18]. Figure 4 shows the DMF vibration reduction characteristics. The engine starter output torque is computed by setting the starter's characteristic curve, and engine excitation torque is computed in the software by setting the tested cylinder pressure curve, which is shown in Figure 5.

Values of parameters, corresponding to Table 1, are listed as follows: $I_1 = 0.00515$ kg·m^2, $I_2 = 0.00978$ kg·m^2, $I_3 = 0.0072$ kg·m^2, $I_4 = 0.0075$ kg·m^2, $I_5 = 0.0081$ kg·m^2, $I_6 =$

angular velocity; and λ_p is the ratio of crank radius to connecting rod length.

The torque produced by cylinder gas pressure, T_g, can be expressed as (assume ignition sequence is 1-3-4-2)

$$T_g = 4[T_0 + a_2\sin(2\zeta t + \varphi_2) + a_4\sin(4\zeta t + \varphi_4) + \cdots],$$ (5)

where T_0 (NM) is the average torque and a_i and φ_i ($i = 2, 4, 6, \ldots$) are the amplitudes and phase angles of the sinusoidal excitations with different orders, respectively.

The engine torque T_Σ can be expressed as $T_\Sigma = T_{rm} + T_g$. For a 4-cylinder 4-stroke engine, the vibration will increase distinctly when the harmonic numbers are 2, 4, 6, . . ., where excitation torque vectors generated by cylinders are with the same phase [12].

The excitation frequency with different orders f (Hz) can be expressed as

$$f = \frac{\gamma \cdot n}{60},$$ (6)

where γ is harmonic number and n (rpm) is crankshaft rotational speed.

3. Modeling and Experiment of DMF Driveline under Start-Up Condition

3.1. DMF Driveline Torsional Vibration Model. An analytical model of driveline torsional vibration system under start-up condition, as shown in Figure 3, is built on the basis of the above analysis and neglecting the influence of engine accessories driven by generator pulley [17]. The model embodies two driveline features during engine start-up: (1) clutch is separated from the gearbox; (2) starter torque (T_m) is exerted on the crankshaft when the engine is started

TABLE 1: Parameters of DMF driveline under start-up condition.

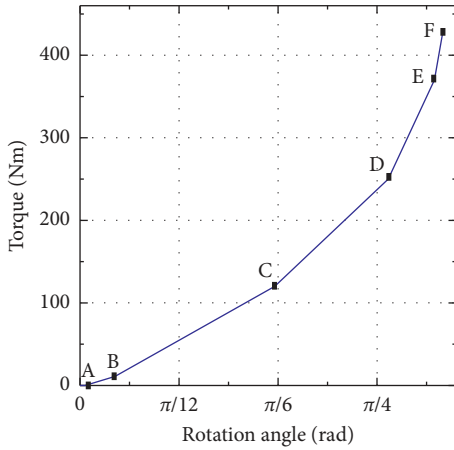| Symbol	Meaning
I_1	Rotary inertia of crankshaft front end absorber outer ring
I_2	Rotary inertia of crankshaft front end absorber inner ring
$I_3 \sim I_6$	Rotary inertia of each crank
I_7	Rotary inertia of DMF primary flywheel
I_8	Rotary inertia of DMF secondary flywheel
I_9	Rotary inertia of clutch cover
K_1	Torsional stiffness of crankshaft front end absorber
K_2	Torsional stiffness of crankshaft front end
K_3	Torsional stiffness between the 1st crank and the 2nd crank
K_4	Torsional stiffness between the 2nd crank and the 3rd crank
K_5	Torsional stiffness between the 3rd crank and the 4th crank
K_6	Torsional stiffness of crankshaft rear end
K_7	Multistage torsional stiffness of DMF
K_8	Torsional stiffness between the 2nd flywheel and clutch cover
C_1	Damping coefficient of crankshaft front end absorber
$C_2 \sim C_5$	Equivalent torsional damping coefficient of each crank
T_{ht}	Hysteresis torque of DMF

FIGURE 4: DMF vibration reduction characteristics.

A (($\pi/240 \pm \pi/360$) rad, (0 ± 2.5) Nm)
B (($53\pi/1800 \pm \pi/90$) rad, (11 ± 10) Nm)
C (($59\pi/360 \pm \pi/60$) rad, (120 ± 15) Nm)
D (($467\pi/1800 \pm \pi/60$) rad, (250 ± 40) Nm)
E (($179\pi/600 \pm \pi/60$) rad, (370 ± 50) Nm)
F (($11\pi/36 \pm \pi/60$) rad, 430 Nm)

0.009 kg·m^2, $I_7 = 0.133 \text{ kg·m}^2$, $I_8 = 0.062 \text{ kg·m}^2$, $I_9 = 0.0781$ kg·m^2, $K_1 = 19519 \text{ Nm/rad}$, $K_2 = 252.7 \times 10^3 \text{ Nm/rad}$, $K_3 = 583.7 \times 10^3 \text{ Nm/rad}$, $K_4 = 581.2 \times 10^3 \text{ Nm/rad}$, $K_5 = 592.6 \times 10^3 \text{ Nm/rad}$, $K_6 = 710.3 \times 10^3 \text{ Nm/rad}$, $K_8 = \infty$ (suppose the 2nd flywheel is connected with clutch cover rigidly), $C_1 = 2 \text{ Nms/rad}$, $C_2 = 0.25 \text{ Nms/rad}$, $C_3 = 0.25 \text{ Nms/rad}$, $C_4 = 0.25 \text{ Nms/rad}$, and $C_5 = 0.25 \text{ Nms/rad}$. The DMF vibration reduction characteristics are shown in Figure 4.
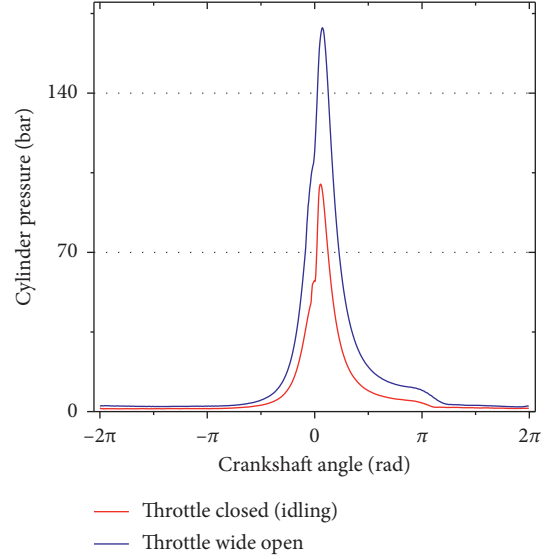

FIGURE 5: Engine cylinder pressure.

3.2. Experimental Validation. A start-up test is conducted in this paper for investigating the driveline vibration characteristics during engine start-up and verifying the validity and accuracy of the research model.

The DMF vibration is acquired by the nonuniform pulse signal of magnetoelectric tachometric transducer during the measurement. Tap a M12 threaded hole on clutch housing (aligned with the flywheel ring gear) and gearbox housing (aligned with the driving gear of the 1st gear pair), respectively. Screw the sensors into the threaded holes until the sensors touch the inner gears. Screw the sensors at the reverse direction for 2 circles for keeping the distance from sensor head to tips of teeth on gears about 3.5 mm, which is among the sensitive distance of sensor testing, 0~5 mm. The other side of sensors is connected with Rotec testing system. Start the test after the equipment installation and debugging. Start the sample vehicle. Maintain for a moment after the vehicle is started successfully. Signals under start-up condition are acquired in the above processes. The data are sent into an integrated laptop from Rotec testing system in real time. "Rotec RASnbk analysis system" in the laptop functions as analyzing the vibration signals, including angular velocity, angular acceleration, angular deflection value, order analysis, etc. Figure 6 shows the sensor installation and testing site.

Figures 7 and 8 depict the speed fluctuation of simulation and test, respectively. Figures 9 and 10 show the DMF angular displacement of simulation and test (analyzed by Rotec RASnbk system) during engine start-up, respectively.

The research model is verified by the comparison of simulated and experimental data of DMF angular velocity fluctuation and angular displacement. Start-up process is separated into 3 phases (Phase A: driven phase; Phase B: transition phase; Phase C: idling phase) for analysis in this paper due to the unsteady state [19] caused by starter torque and engine ignition. The crankshaft is driven by starter in Phase A, where the major excitation is from the capsizing
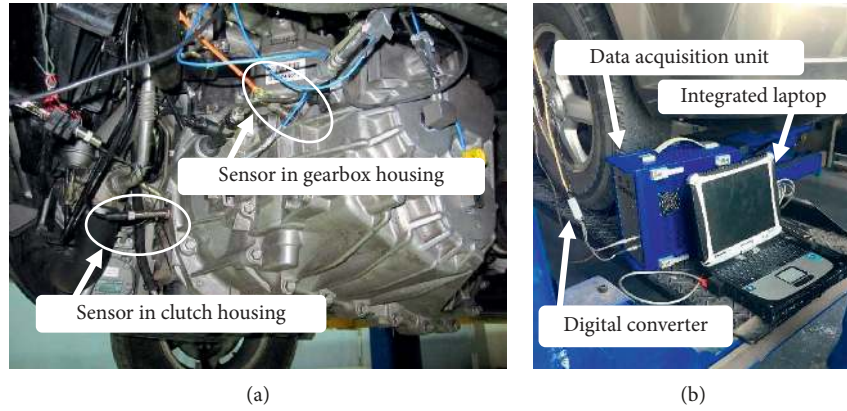
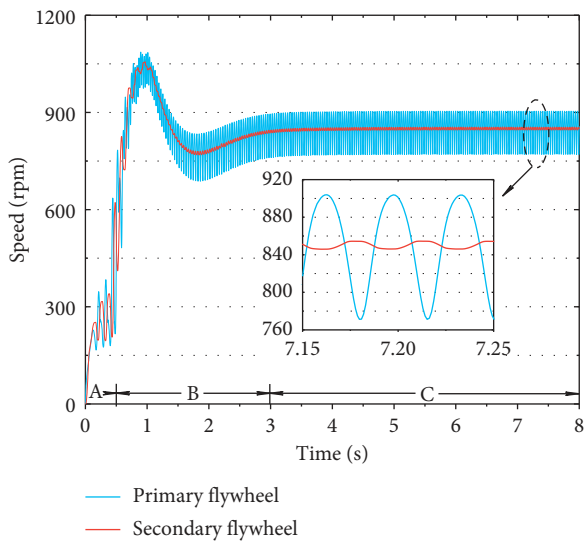Figure 6: (a) Sensor installation and (b) testing site.
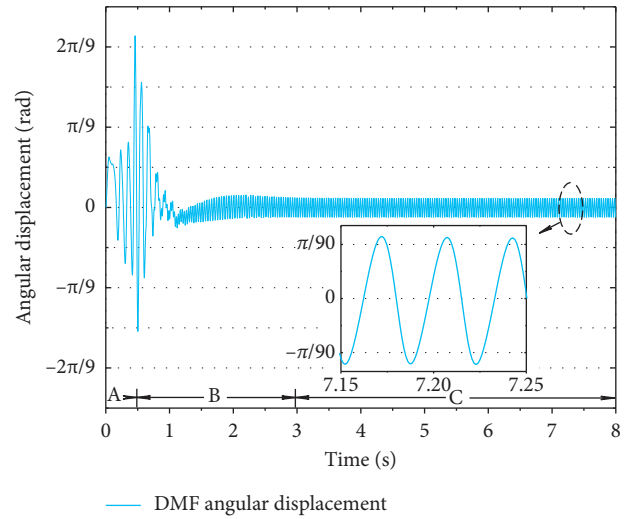

Figure 7: Simulating speed fluctuation.

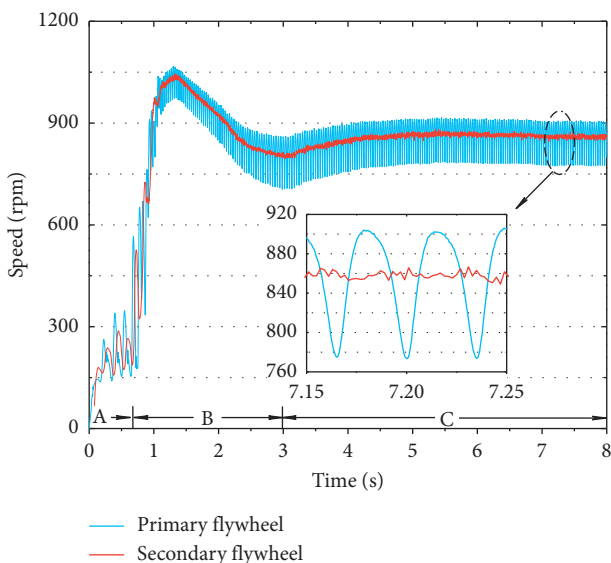Figure 9: Simulating DMF angle displacement.

Figure 8: Testing speed fluctuation.

moment induced by crankshaft reaction force and cylinder pressure. The starter will be disengaged from flywheel ring gear, and the system vibration is mainly caused by combustion excitation after the engine ignition. Compared to Figure 8, the variation trend and fluctuation amplitude of engine speed in Figure 7 exhibit good agreement with the experimental data. Resultantly, effective input excitations can be provided for the driveline vibration system.

Suppose the relative rotation angle of DMF is calculated by the absolute value of rotation angle, the speed fluctuation amplitude is calculated by the difference between peak value and valley value of the speed. The comparison between simulation and experiment data and relative errors (suppose relative error = (simulation value − test value)/test value) is listed in Table 2.

Table 2 implies that the model simulates the DMF relative rotation angle and vibration control effect in start-up with a reasonable accuracy. The errors are mainly induced by neglecting gearbox's inertial in the model, uncertain damping of driveline and the discrepancy between designed characteristics of DMF (e.g., DMF damping values, which
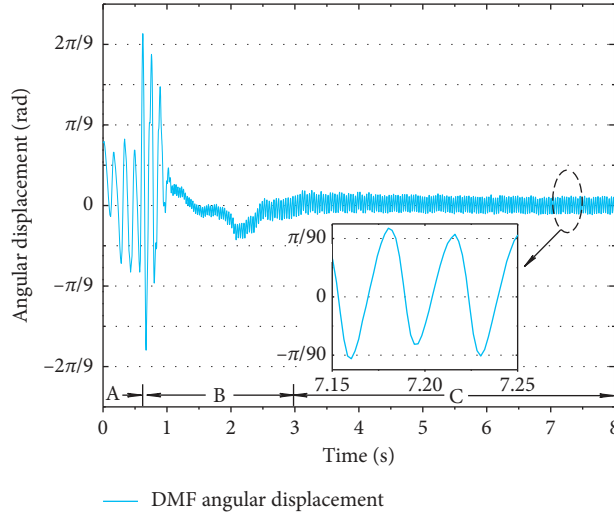
FIGURE 10: Testing DMF angle displacement.

TABLE 2: Simulation and test data comparison and relative errors.

Phase		Max. relative angle (rad)	Angle error (%)	Max. speed fluctuation amplitude (rpm)	Amplitude error (%)
A	Simulation	0.0936π	+2.1	133.5	+7.4
	Test	0.0917π		124.3	
B	Simulation	0.2378π	+0.7	210.6	+3.4
	Test	0.2361π		203.7	
C	Simulation	0.0126π	−3.8	8.5	−5.6
	Test	0.0131π		About 9	

cannot be easily controlled) and the characteristics after DMF installation. In conclusion, the research model is valid for further studies.

4. DMF Characteristic Analysis Based on Vibration Control in Start-Up

According to the simulation and test results above, speed fluctuation of the secondary flywheel is distinct in Phase A, where the amplitude is about 100~150 rpm. Larger oscillation occurs in Phase B, where the maximum torsion angle of DMF is about 0.23 rad around 300~600 rpm since the system is passing through the resonance speed zone. Hence, Phase B is the significant stage of vibration control [20]. When the speed is stabilized at around 850 rpm, the fluctuation amplitude of engine speed is inhibited from 130 rpm to about 10 rpm, exhibiting comparatively good vibration attenuation effect.

The relation between DMF characteristics and vibration control effect is investigated and analyzed in this chapter based on the proposed research model, which can prescribe the design requirements under start-up condition for DMF matching.

4.1. Analysis of DMF Rotary Inertia Distribution. The total rotary inertia of DMF should be equal to the total rotary inertia of the engine single flywheel [21] for maintaining the effect of energy storage. Suppose the clutch cover is connected with the secondary flywheel rigidly, the sum of I_7, I_8, and I_9 is constrained as a constant. In this paper, the ratio of rotary inertia, μ, is defined as: $\mu = I_7/(I_8 + I_9)$.

The DMF vibration control effect is evaluated separately on account of the different vibration characteristics in Phases A, B, and C. The engine side vibration is considered as one of the evaluation criteria, since the DMF rotary inertia distribution also effects the vibration of engine side [22].

Phase A (about 0~0.4 s): Figure 11 depicts the time-domain angular acceleration of the primary flywheel and the secondary flywheel under different μ values. Phases B and C (after 0.4 s): Figure 12 shows the 2nd order values of angular acceleration of the primary flywheel and the secondary flywheel under different μ values, which can also embody time feature.

Analyze the vibration attenuation performance of DMF under different μ values. Phase A (about 0~0.4 s): the maximum absolute values of the primary flywheel angular acceleration (a_{A1max}) and the secondary flywheel angular acceleration (a_{A2max}) are utilized as evaluation parameters. Phase B (about 0.4 s~3 s): the maximum values of the 2nd order angular acceleration of primary flywheel (a_{B1max_O2}) and secondary flywheel (a_{B2max_O2}) are used as evaluation parameters. Phase C (after 3 s): the averages of the 2nd order angular acceleration of primary flywheel (a_{C1ave_O2}) and secondary flywheel (a_{C2ave_O2}) are utilized as evaluation parameters on account of the stable speed in Phase C. The evaluation parameters are summarized in Table 3, where the attenuation degree γ is defined as γ = (value of the primary
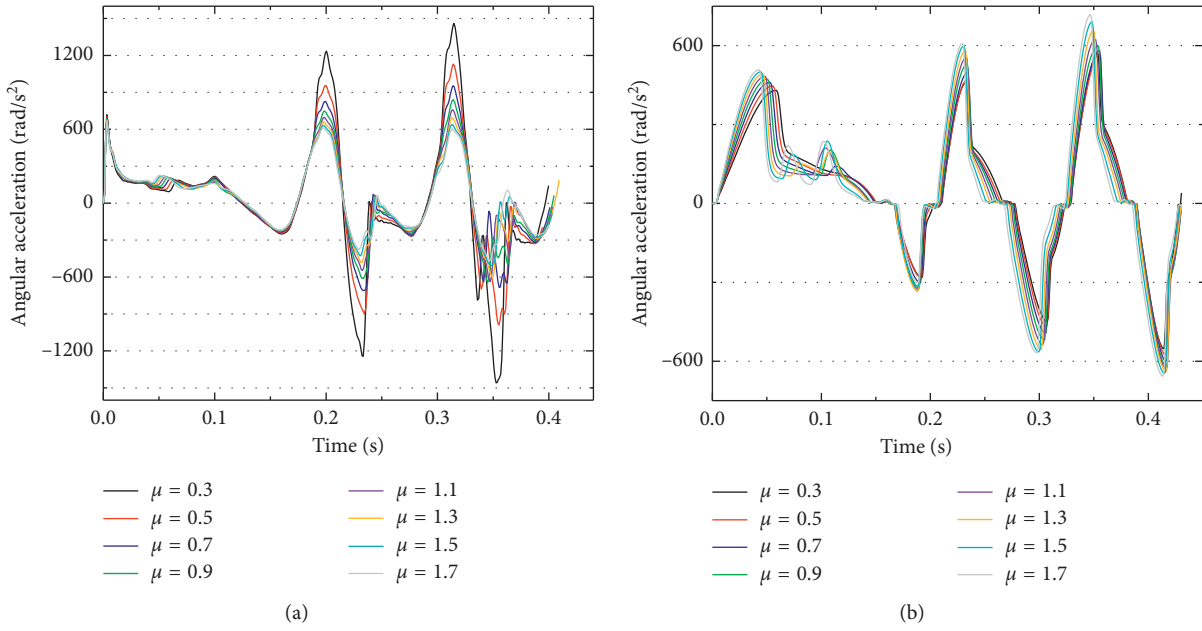
FIGURE 11: Angular acceleration under different μ values in Phase A. (a) The primary side result; (b) the secondary side result.
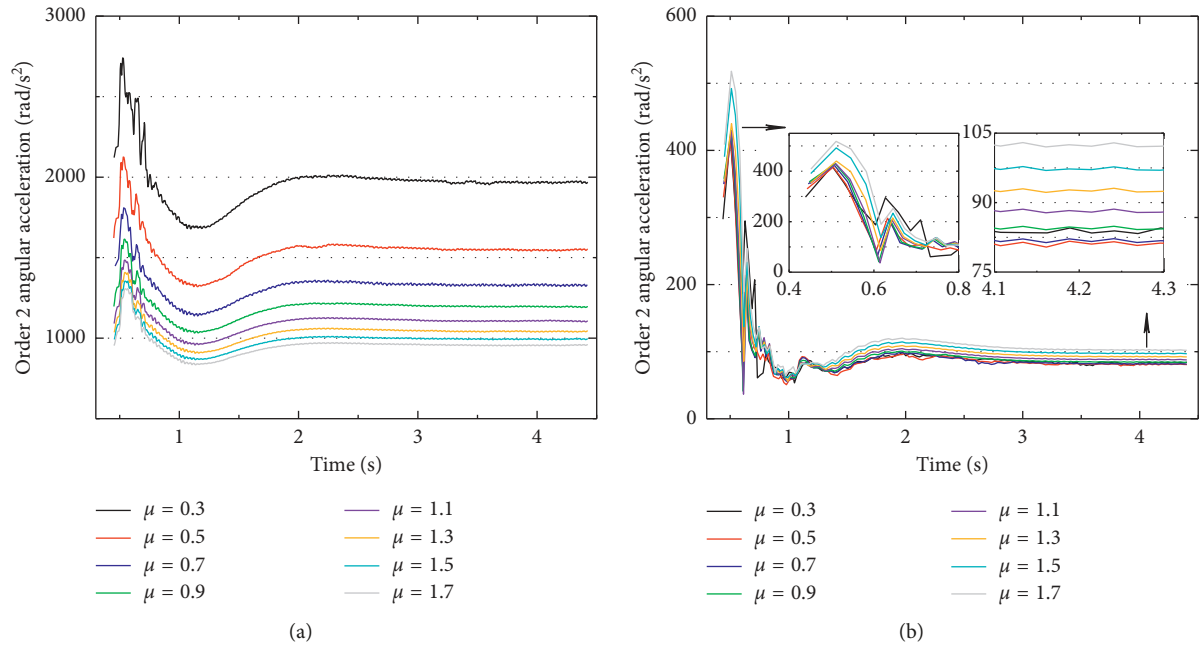

FIGURE 12: The 2nd order angular acceleration under different μ values in Phases B and C. (a) The primary side result; (b) the secondary side result.

TABLE 3: DMF vibration control performances under different μ values.

μ	0.3	0.5	0.7	0.9	1.1	1.3	1.5	1.7
a_{A1max} (rad/s^2)	1460.5	1129.8	953.3	840.8	757	693.2	639.3	600
a_{A2max} (rad/s^2)	569.8	575.8	600.3	621.1	631	658.4	691.8	719.1
γ	0.61	0.49	0.37	0.26	0.166	0.05	-0.08	-0.2
a_{B1max_O2} (rad/s^2)	2740.2	2124.8	1809	1614.3	1485	1408.2	1355	1308
a_{B2max_O2} (rad/s^2)	419.8	415.9	423.3	430	429	440	492.2	518
γ	0.85	0.8	0.77	0.73	0.71	0.69	0.64	0.6
a_{C1ave_O2} (rad/s^2)	1968.4	1550.3	1328.3	1193.8	1104.7	1041	994.8	957.8
a_{C2ave_O2} (rad/s^2)	83.3	81.4	82.4	85	88.7	93	97.9	103
γ	0.96	0.95	0.94	0.93	0.92	0.91	0.9	0.89

flywheel evaluation parameter – value of the secondary flywheel evaluation parameter)/value of the primary flywheel evaluation parameter.

Table 3 indicates that the secondary flywheel vibration declines and the DMF performance becomes worse successively when μ varies from 0.3 to 1.7. However, intense oscillation occurs at the engine side when μ is too small. Simultaneously, the engine vibration will be even amplified in Phase A and the 2nd order vibration amplitude of the secondary flywheel is large in Phases B and C when μ is too large. In conclusion, the optimum selection range of μ is 0.7~1.1.

4.2. Analysis of DMF Hysteresis Torque. Generally, vibrational energy is converted into thermal energy by damping in mechanical systems. Frictional damping of normal DMF, consuming mechanical energy for attenuating driveline vibration, is a critical kinetic parameter of DMF. For DMF-CSS (DMF with circumferential short springs) [23, 24] in this paper, in addition to damping mechanism, the DMF damping is also provided by the friction between spring seat and spring seat track, lubricating grease, and the friction between spring seats. DMF exhibits nonlinear damping characteristics because the centrifugal force of springs increases with the speed increment and spring seats wedge against each other in large torsion angle zone, inducing the augment of friction. DMF damping characteristic is manifested by the hysteresis effect in DMF measurement [25], hence the DMF damping characteristic is represented by hysteresis torque (T_{ht}) in this paper. Five schemes of DMF hysteresis property shown in Table 4 are designed for investigating the requirements for DMF damping characteristic in start-up process.

Phase A (about 0~0.4 s): Figure 13 shows the time-domain angular acceleration of the primary flywheel and the secondary flywheel under different damping schemes. Phases B and C (after 0.4 s): Figure 14 shows the 2nd order angular acceleration of the primary flywheel and the secondary flywheel under different damping schemes with time feature.

According to the analysis principle in Section 4.1, the DMF vibration control performances under different damping schemes are listed in Table 5.

It can be inferred from Table 5 that DMF damping characteristic imposes little effect on the engine side vibration, according to a_{A1max}, a_{B1max_O2}, a_{C1ave_O2}. Attenuation degrees in Phases A and B increase and the secondary flywheel vibration declines successively with the increase of DMF damping. With small damping of DMF, good vibration control performance is shown in Phase C. In conclusion, small damping is required in the interval of DMF small torsion angle, corresponding to idling condition Phase C, while large damping is demanded in the interval of large torsion angle for inhibiting vibration, corresponding to Phases A and B. For this paper, based on the DMF attenuation effect under start-up condition, the recommended hysteresis torque from point A to point E is ±0.25 Nm, ±5 Nm, ±20 Nm, ±50 Nm, and ±60 Nm, respectively.

4.3. Analysis of DMF Torsional Stiffness. Except for transmitting the maximum torque of engine, DMF is demanded to bear instantaneous impact loads in driveline. Therefore, the maximum torque that the torsional springs can withstand should be designed as at least 1.3 times the maximum torque of engine for ensuring the DMF torque reserve capacity [1]. Moreover, the maximum torsional angle of ordinary DMF is about $\pi/6$~$\pi/3$ rad. Therefore, the design of DMF piecewise torsional stiffness is restricted by torque and DMF rotation angle, and the stiffnesses restraint with each other.

The torsional stiffness of DMF is generally divided into three stages. The 1st stage stiffness is the smallest and utilized in engine idling, making the driveline natural frequency lower than the idle excitation frequency of engine. The 2nd stage stiffness is used in driving condition, and driveline natural frequency can be avoided from the engine excitation frequency band corresponding to the common speed of engine. The 3rd stage stiffness is the largest and utilized for attenuating the oscillation caused by rapid change of load in driveline. The DMF in this paper is designed with five-stage torsional stiffness originally. For researching the relation between DMF torsional stiffness and vibration absorption performance, the first four stages of stiffness are discussed according to the range of torsion angle that DMF works in under start-up condition. Suppose the angles of inflection points of stiffness remain unchanged, 4 schemes of DMF stiffness (stf.) characteristic shown in Figure 15 and Table 6 are designed.

The DMF vibration control performances of 4 schemes are compared as shown in Figures 16 and 17.

The evaluation parameters are summarized in Table 7.

According to a_{A1max}, a_{B1max_O2}, and a_{C1ave_O2}, stiffness property of DMF imposes little effect on the vibration of engine side. For the 4 schemes, Phases A, B, and C show the similar result that the smaller the stiffness values of the first three stages are, the better the DMF vibration control effect is, namely, the secondary flywheel vibration is smaller and attenuation degree γ is larger. Resultantly, the design requirement for DMF stiffness in start-up is that torsional stiffness of DMF should be as low as possible for attenuating the resonance oscillation and optimizing the vibration under engine idle condition. For this paper, based on the vibration control effect of DMF under start-up condition, the design of piecewise stiffness is recommended as 44.1 Nm/rad, 181.1 Nm/rad, 366.4 Nm/rad, 1473.3 Nm/rad, and 2644.4 Nm/rad, respectively.

5. Summary and Conclusion

This paper established the driveline torsional oscillation model under start-up condition that considers starter excitation, engine cylinder excitation, and DMF, and the vehicle start-up experiment was conducted. The influence of DMF kinetic parameters on driveline oscillation during engine start-up was carried out, providing the design requirements and references under start-up condition for DMF matching.

TABLE 4: Schemes of DMF hysteresis torque design.

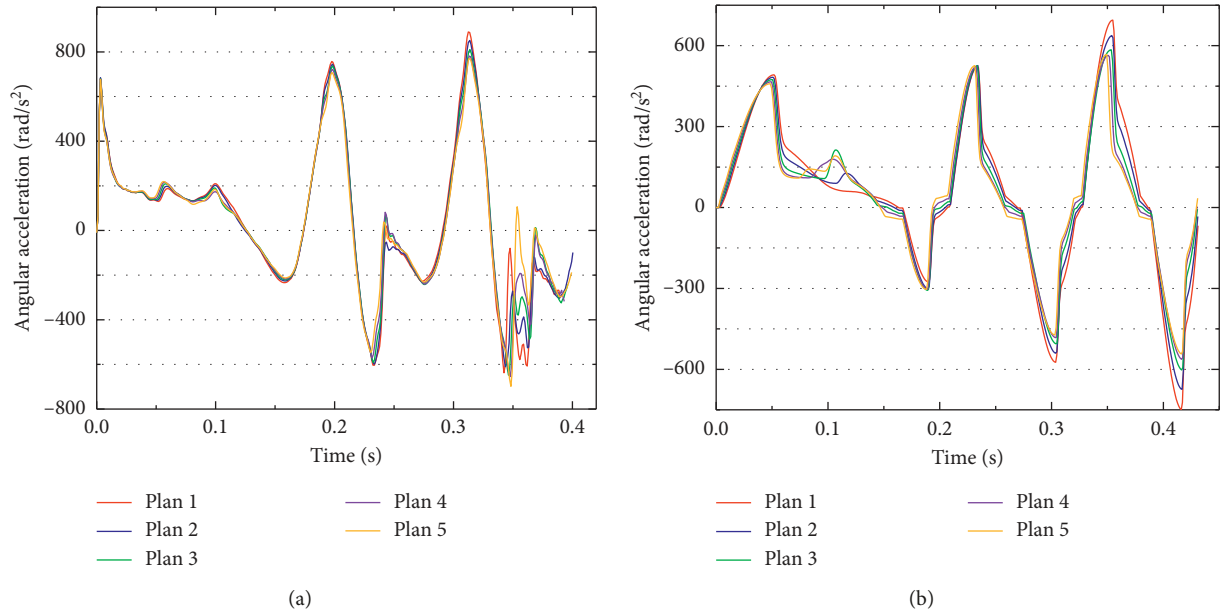| Angle (rad)	Scheme 1 T_{ht} (Nm)	Scheme 2 T_{ht} (Nm)	Scheme 3 T_{ht} (Nm)	Scheme 4 T_{ht} (Nm)	Scheme 5 T_{ht} (Nm)
$\pi/240$	±0.25	±1.5	±3	±4.5	±6
$53\pi/1800$	±5	±7.5	±10	±12.5	±15
$59\pi/360$	±10	±12.5	±15	±17.5	±20
$467\pi/1800$	±30	±35	±40	±45	±50
$179\pi/600$	±40	±45	±50	±55	±60

FIGURE 13: Angular acceleration under different damping schemes in Phase A. (a) The primary side result; (b) the secondary side result.
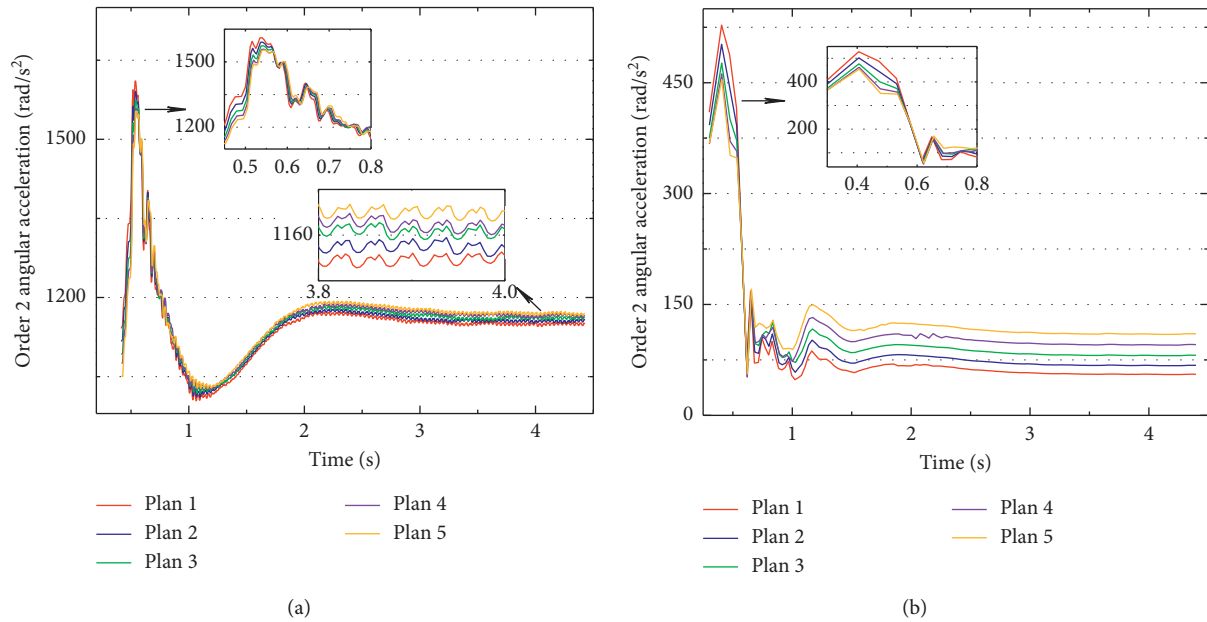

FIGURE 14: The 2nd order angular acceleration under different damping schemes in Phases B and C. (a) The primary side result; (b) the secondary side result.

TABLE 5: DMF vibration control performances under different damping schemes.

	Scheme 1	Scheme 2	Scheme 3	Scheme 4	Scheme 5
a_{A1max} (rad/s^2)	889.6	851.4	810.6	781.4	770
a_{A2max} (rad/s^2)	748.9	674.1	602.2	564.1	567.4
γ	0.158	0.208	0.257	0.278	0.263
a_{B1max_O2} (rad/s^2)	1610.8	1590.4	1573.8	1558.2	1554.1
a_{B2max_O2} (rad/s^2)	527.8	501.9	476.5	462	454.1
γ	0.672	0.684	0.697	0.703	0.708
a_{C1ave_O2} (rad/s^2)	1149.3	1155.9	1161.4	1164.6	1167.7
a_{C2ave_O2} (rad/s^2)	55.6	68.3	81.9	96.2	110.7
γ	0.952	0.941	0.929	0.917	0.905
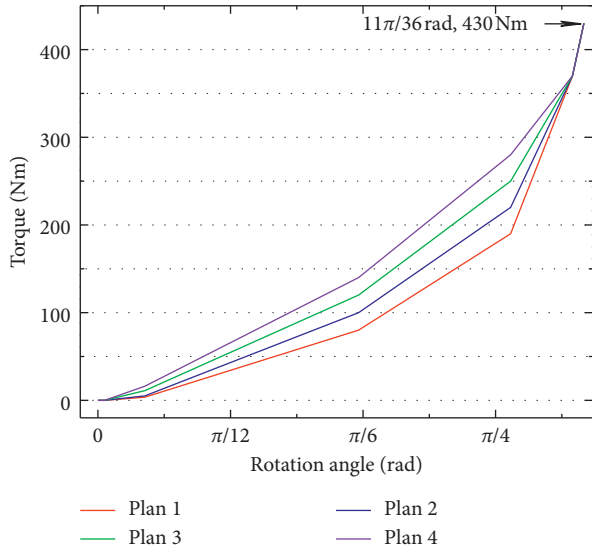
FIGURE 15: Schemes of DMF stiffness design.

TABLE 6: Stiffness values of four schemes.

	Plan 1	Plan 2	Plan 3	Plan 4
1st stf.	44.1	63.0	138.5	201.5
2nd stf.	181.1	224.9	258.1	293.6
3rd stf.	366.4	399.7	433.0	466.4
4th stf.	1473.3	1227.8	982.2	736.7
5th stf.	2644.4	2644.4	2644.4	2644.4

Note: the unit of stiffness is Nm/rad.

The following conclusions have been drawn from this paper:

(1) The simulation and experiment results demonstrate the large speed fluctuation of DMF in Phase B, where the system is passing through the resonance speed zone. By comparing with the experimental results, the proposed model that considers excitations of
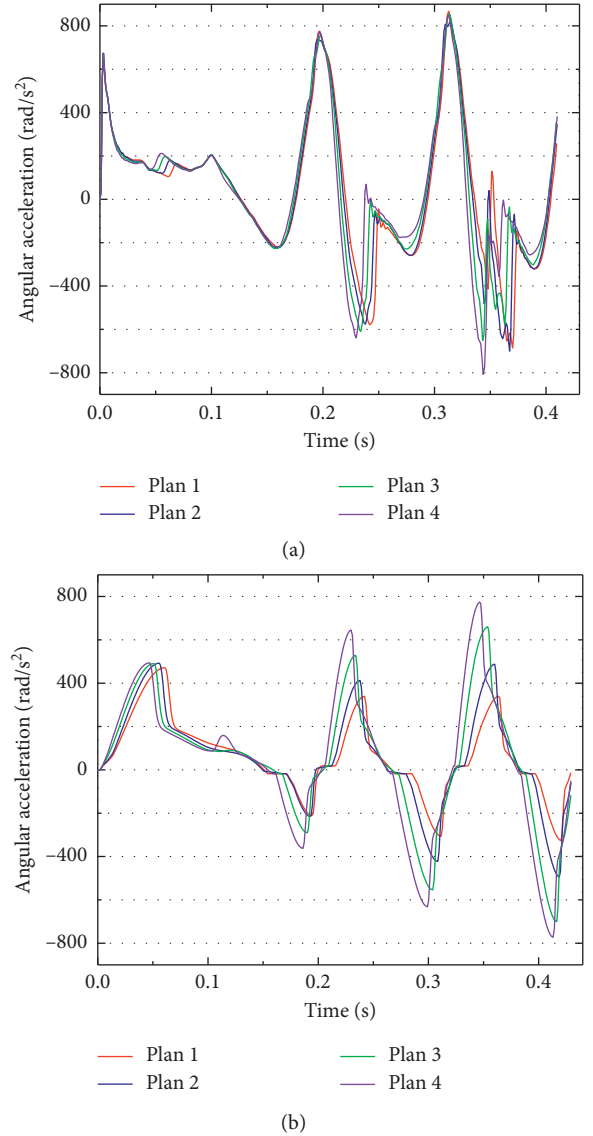

(a)

(b)

FIGURE 16: Angular acceleration of different stiffness schemes in Phase A. (a) The primary side result; (b) the secondary side result.

starter and engine is verified to simulate the vibration control effect of DMF in start-up validly.

(2) Rotary inertia ratio (μ) of DMF imposes a significant effect on engine vibration, and the primary flywheel will vibrate furiously if μ is too small. The vibration from engine will be even amplified in Phase A, and the 2nd order vibration amplitude is large in Phases B and C when μ is too large. As a result, for reaching a good vibration control effect during start-up, the optimum range of μ is 0.7~1.1.

(3) Damping and stiffness characteristics of DMF impose little effect on the vibration at engine side. For start-up condition, small damping is required in the range of small DMF angle, while large damping is required in the range of large angle. The recommended hysteresis torque from point A to point E is ±0.25 Nm, ±5 Nm, ±20 Nm, ±50 Nm, ±60 Nm,
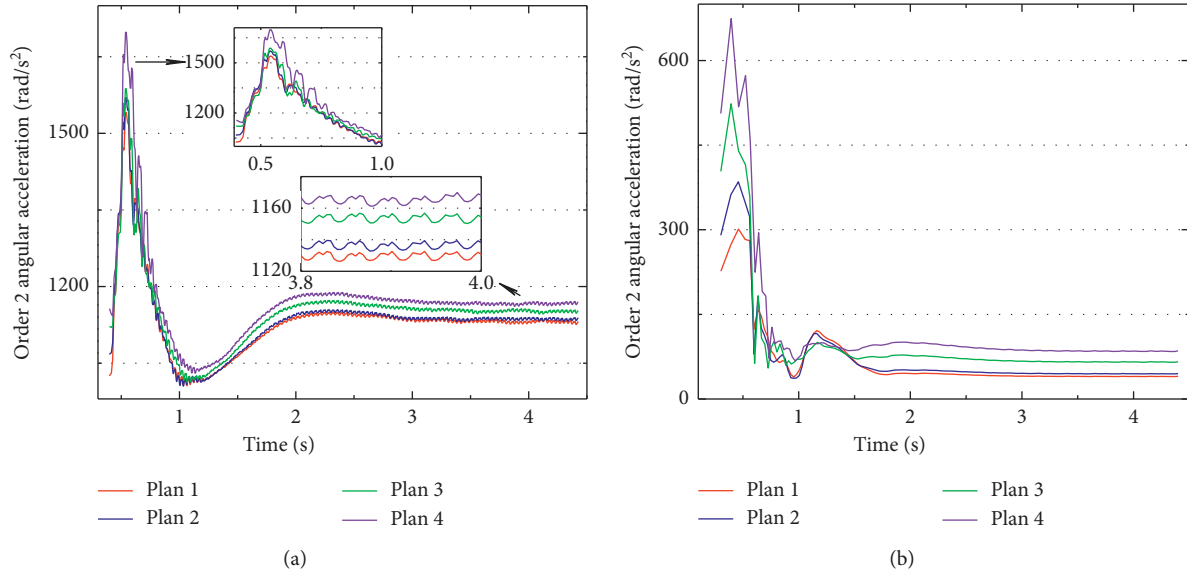
FIGURE 17: The 2nd order angular acceleration under different stiffness schemes in Phases B and C. (a) The primary side result; (b) the secondary side result.

TABLE 7: DMF vibration control performances under different stiffness schemes.

	Plan 1	Plan 2	Plan 3	Plan 4
a_{A1max} (rad/s^2)	867.2	819.2	856.9	850.2
a_{A2max} (rad/s^2)	339.8	495	704	775.7
γ	0.608	0.396	0.178	0.088
a_{B1max_O2} (rad/s^2)	1540.7	1570.3	1587.6	1697.8
a_{B2max_O2} (rad/s^2)	301.3	385	523.4	674.3
γ	0.804	0.755	0.67	0.603
a_{C1ave_O2} (rad/s^2)	1129.9	1136.4	1152.5	1166.9
a_{C2ave_O2} (rad/s^2)	39.9	44.7	65.6	84.7
γ	0.965	0.96	0.943	0.927

respectively. Torsional stiffness of DMF should be as low as possible. The recommended design of piecewise stiffness is 44.1 Nm/rad, 181.1 Nm/rad, 366.4 Nm/rad, 1473.3 Nm/rad, and 2644.4 Nm/rad, respectively.

Data Availability

The data used to support the findings of this study are available from the corresponding author upon request.

Conflicts of Interest

The authors declare that there are no conflicts of interest regarding the publication of this paper.

Acknowledgments

References

[1] L. Wei, *Research on the method and the performance of isolation of torsional vibration of DMF-CS based on the vehicle power train*, Ph.D thesis, Jilin University, Changchun, China, 2009.

[2] C. F. Lü, "The characteristic study on torsion vibration of dual mass flywheel and its simulation analysis," Master thesis, Shanghai Jiao Tong University, Shanghai, China, 2008.

[3] L. Wei and W. K. Shi, "Summary of studies on dual mass flywheel (DMF)," *Noise and Vibration Control*, vol. 28, no. 5, pp. 1–5, 2008.

[4] A. Walter, C. Lingenfelser, U. Kiencke, S. Jones, and T. Winkler, "Cylinder balancing based on reconstructed engine torque for vehicles fitted with a dual mass flywheel (DMF)," *SAE International Journal of Passenger Cars-Mechanical Systems*, vol. 1, no. 1, pp. 810–819, 2008.

[5] U. Schaper, O. Sawodny, U. Blessing, and T. Mahl, "Modeling and torque estimation of an automotive dual mass flywheel," in *Proceedings of American Control Conference*, pp. 1207–1212, St. Louis, MO, USA, June 2009.

[6] J. Kim, "Launching performance analysis of a continuously variable transmission vehicle with different torsional couplings," *Journal of Mechanical Design*, vol. 127, no. 2, pp. 295–301, 2005.

[7] A. Fidlin and R. Seebacher, "DMF simulation techniques," in *Proceedings of 8th LuK Symposium*, pp. 55–71, Bavaria, Germany, May 2006.

[8] M. Zink and M. Hausner, "LuK clutch systems and torsional dampers," in *Proceedings of Schaeffler Symposium*, pp. 8–27, Bavaria, Germany, 2010.

[9] J. J. Hu, D. T. Qin, Y. S. Zhao et al., "Study on natural torsional vibration characteristics of dual mass flywheel-radial spring type torsional vibration damper," *China Mechanical Engineering*, vol. 19, no. 15, pp. 1800–1805, 2008.

[10] H. B. Schweinfurt, "Systematic search for and vibratory assessment of new action principles for alternative rotary vibration decoupling systems in the passenger car driveline," *Drive System Technique*, no. 6, pp. 3–12, 2004.

[11] D. M. Chen, Z. Huang, C. Ling et al., "Torsion stiffness calculation and optimization design of arc helix spring of DMF," *China Mechanical Engineering*, vol. 21, no. 14, pp. 1676–1682, 2010.

[12] Y. Wang, X. Qin, S. Huang et al., "Design and analysis of a multi-stage torsional stiffness dual mass flywheel based on vibration control," *Applied Acoustics*, vol. 104, pp. 172–181, 2016.

[13] S. Deng and R. Burde, "Evaluation of interdependent behavior of dual mass flywheel (DMF) and engine starting system," in *Proceedings of SAE Technical Paper Series*, No. 2010-01-0188, Warrendale, PA, USA, 2010.

[14] Z. Y. Chen, Y. Mao, W. K. Shi et al., "Research on torsional vibration of powertrain with dual mass flywheel in start-stop conditions," *Journal of Beijing Institute of Technology*, vol. 36, no. 1, pp. 42–47, 2016.

[15] M. Mitschke and H. Wallentowitz, *Dynamik der Kraftfahrzeuge*, Springer Fachmedien Wiesbaden Press, Wiesbaden, Germany, 2014.

[16] G. Genta, *Torsional Vibration of Crankshafts*, Springer US Press, New York, NY, USA, 2009.

[17] L. Chen, *Reseach on dynamic characteristics of passenger car dual mass flywheel*, Ph.D thesis, Wuhan University of Technology, Wuhan, China, 2009.

[18] Z. Zhen, G. Xiang, P. Daoyuan et al., "Study on the control strategy of shifting time involving multigroup clutches," *Mathematical Problems in Engineering*, vol. 2016, Article ID 9523251, 17 pages, 2016.

[19] T. Wellmann, K. Govindswamy, and D. Tomazic, "Integration of engine start/stop systems with emphasis on NVH and launch behavior," *SAE International Journal of Engines*, vol. 6, no. 2, pp. 1368–1378, 2013.

[20] L. Li and R. Singh, "Start-up transient vibration analysis of a vehicle powertrain system equipped with a nonlinear clutch damper," *SAE International Journal of Passenger Cars-Mechanical Systems*, vol. 8, no. 2, pp. 726–732, 2015.

[21] Y. D. Lu, "The study of multistage non-linear dual mass flywheel damper," Master thesis, Jilin University, Changchun, China, 2008.

[22] Y. Ding, *Automotive friction clutch torsional vibration damper characteristics and parametric analysis*, Ph.D thesis, Changchun University of Science and Technology, Changchun, China, 2009.

[23] A. Kooy, A. Gillmann et al., "DMFW-nothingnew," in *Proceedings of 7th LuK Symposium*, Bühl, Germany, April 2002.

[24] A. Albers, "Advanced development of dual mass flywheel (DMFW) design-noise control for today's automobiles," in *Proceedings of 5th LuK Symposium*, Bühl, Germany, 1994.

[25] Y. chen, "Performance analysis of powertrain NVH considering the dynamic characteristics of dual mass flywheel," Master thesis, Chongqing University of Technology, Chongqing, China, 2017.